JOURNAL OF THERMOPHYSICS AND HEAT TRANSFER
Vol. 10, No. 4, October–December 1996

Theoretical Analysis for Mechanical Erosion of Carbon-Base Materials in Ablation

Fen Ren*
Chinese Academy of Sciences, Beijing 100080, People's Republic of China
and
H. S. Sun† and L. Y. Liu‡
China Academy of Launch Vehicle Technology, Beijing 100076, People's Republic of China

This article derives and provides a theoretical analysis for the mechanical erosion of carbon-base materials in ablation. The theory of mechanical erosion based on a nondimensional critical roughness parameter is proposed. The important parameters in this analytical method are independent of the test. The analysis accounts for the heating, pressure, and shear forces acting on material particles exposed to the boundary-layer flow. For the validity of a theoretical analytical method a computational example is given. The theoretical results agree fairly with the experimental data.

Nomenclature

a = characteristic height of ablated filler particle
C_f = skin friction coefficient
d = particle size
h = height of exposed filler particle
h_s = equivalent sand roughness
$\bar{M}$ = average molecular weight of gas phase at wall
$\dot{m}$ = mass loss rate
p = static pressure
Q = drag force
R = universal gas constant
S = surface recession rate
T = wall temperature
t = time
u_e = boundary-layer-edge velocity
x = surface distance
β = fraction of particle surface attached to surrounding matrix
ΔS = surface recession
ρ = surface density of heat shield
ρ_e = density at boundary-layer edge
ρ_w = gas density at wall
σ = tensile stress
σ_u = ultimate strength of particle–matrix bound

Subscripts
b = binder material
c = based on thermochemical mass removal rate of carbon element
ch = based on thermochemical ablation theory
cr = point of filler particle removal
f = filler material
m = maximum value
me = based on mechanical erosion theory
to = total

Presented as Paper 95-2130 at the AIAA 30th Thermophysics Conference, San Diego, CA, June 19–22, 1995; received Aug. 24, 1995; revision received Jan. 20, 1996; accepted for publication Feb. 7, 1996.

*Associate Professor, LHD Institute of Mechanics.
†Senior Engineer.
‡Professor.

Introduction

THE carbon-base materials, such as carbon-phonemic, graphite, and three-dimensional carbon–carbon are considerably interesting ablative materials for re-entry vehicle heat shields. This interest stems from the resistance of carbon-base materials to ablation, its ability to sustain extremely high surface temperatures and reradiate a large amount of energy, and its strength at high temperature. Comparisons of the thermochemical ablative calculative results of the carbon-base materials with the experimental data have revealed discrepancies, particularly at the more severe environmental conditions. The major discrepancy between thermochemical ablative calculation and experimental data is caused by the mechanical erosion (i.e., particulate removal). All carbon-base materials exhibit microscopic spallation, characterized by high frequencies and small particles unresolved with conventional photographic techniques. The analytical methods for the particle removal of carbon-base materials are proposed by studies of predecessors.[1–3] The important parameters in those analytic methods are determined experimentally. A theoretical calculation method is derived in the present study, in which the parameters are independent of tests.

A large body of ground and flight test data exists that indicates that ablative charred surfaces undergo mechanical as well as thermochemical ablation when exposed to severe environments of heating, pressure, and shear forces. This phenomenon has been observed for a wide variety of heat-shield materials, through a combination of analysis and measured recession as well as from direct observation of the ablation phenomena from high-quality motion pictures and scanning electron photomicrographs (or computer tomography). Thermomechanical ablation, or erosion, is the result of both external and internal forces operating on the material surface and char regions. The external forces include aerodynamic shear, high surface pressures, pressure gradients, and drag forces. Internal forces include pressure differences resulting from pyrolysis gases flowing through the char and thermally induced stresses. The important forces are generally regarded to be combinations of the previous text. The prediction technique developed in this study was based on a phenomenological approach to the problem, combining the material test observations with simple analytical models of the erosion mechanism. Although the analysis procedure was developed for graphite, it is generally applicable to other charring or carbon–phenodic composite materials, such as three-dimensional carbon–carbon materials.

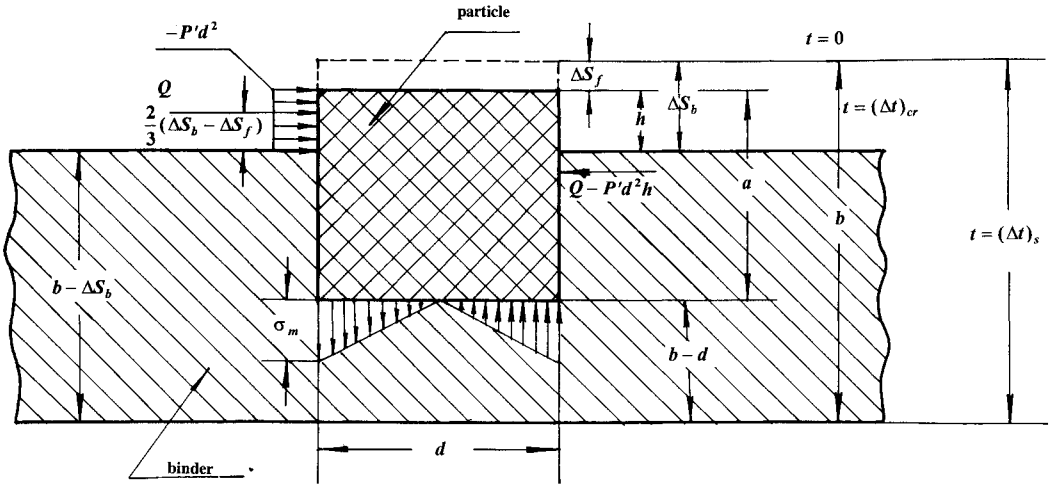

Fig. 1 Particle subjected to aerodynamic forces.

Mechanism of the Particle Erosion for Carbon-Base Materials and Analytical Method

The word particle is used for any solid mass that departs from the ablating surface. Depending on the material under discussion, this particle may be more aptly described as a protuberance, patch, laminate, fiber bundle, radial, or reinforcement. The microscopic particle can only be described in detail after considering the orientation of the material substructure relative to the force field. High-shear tip ablation rates for a family of three materials (carbon phenolic, bulk graphite, and three-dimensional carbon–carbon) exhibit similar small particle erosion characteristics.

1) All materials exhibit microscopic spallation, characterized by high frequencies and small particles unresolved with conventional photographic techniques.

2) All materials have carbon, graphite, or graphitized resin serving as the reinforcements and/or matrix (binder and filler for bulk graphite).

3) All materials exhibit differential ablation between reinforcement and matrix (filler and binder).

4) All materials exhibit surface roughness during the ablation process.

The particulate removal theory based on a nondimensional critical roughness parameter is proposed. It is assumed that mechanical erosion is principally the result of aerodynamic forces acting on protruding particles. The aerodynamic forces arise primarily from surface pressure gradient and rough surface shear, and this rough surface shear is almost entirely because of the drag exerted on individual protuberances. In the following, a simple expression for rough surface skin friction is first developed from published data, and then an idealized model of a protuberant particle is used to derive an equation for the mechanically eroded fraction. For example, the graphite consists of dense filler particles held together by less dense binder matrix containing a certain amount of porosity. The ablation process is assumed to proceed as follows. Initially, the surface is smooth and undergoes thermochemical ablation (see Fig. 1). The filler particle of initial characteristic size d is receding at a rate

$$\dot{S}_f = \Delta S_f/\Delta t = \dot{m}_f/\rho_f \tag{1}$$

and the binder is receding at a rate

$$\dot{S}_b = \Delta S_b/\Delta t = \dot{m}_b/\rho_b \tag{2}$$

where ΔS_f is the surface recession of the particle, and ΔS_b is the surface recession of the binder.

It is assumed that $\dot{m}_f$ will be approximately equal to $\dot{m}_b$ (i.e., equal to $\dot{m}_c$ thermochemical mass removal rate of carbon). This assumption is necessary in the calculation of thermochemical ablation because the thermochemical mass ablation rate of particle carbon and binder carbon is unequal when viewed microscopically[3,5,6] (because of the unequal reactionary rate of two carbons). Up to now in thermochemical ablation calculations for carbon-base materials it has traditionally been assumed that structurally, carbon-base materials are homogeneous materials, in that it consists of a single chemical element: carbon. Thereby ρ_b will be less than ρ_f; therefore, the recession rate of the binder will be greater than that of the filler particle and the filler particle will, with time, become more and more exposed.

The nondimensional roughness height h/a (i.e., the percentage of filler particle exposed) will grow until it reaches some critical value $(h/a)_{cr}$ when the exposed particle can no longer withstand the pressure forces, shear stresses, and subsurface pressures caused by in-depth sublimation. Note that when the environment (e.g., pressure, pressure gradient, and shear) is mild, a critical roughness may not occur. Also, if thermochemical ablation is very low a critical roughness may not develop.

The critical roughness is assumed to develop at a time, $(\Delta t)_{cr}$, when the particles are torn away from the surface, either clean, or with some binder material. Since the amount of binder carried with the stripped particle greatly affects the mass removal rate, two models are presented that are felt to bracket the possibilities. Model A assumes that the particle is stripped clean with no binder attached, and model B assumes that the particle carries with it the complete layer of material to the bottom of the grain, whereupon the process repeats itself.

The ratio of roughness height h to surface particle size a, after time Δt, is

$$h/a = (\Delta S_b - \Delta S_f)/(d - \Delta S_f) \tag{3}$$

and at critical time $(\Delta t)_{cr}$, is

$$(\Delta t)_{cr} = \left[\frac{\rho_f}{\rho_b} + \left(\frac{h}{a}\right)_{cr} - 1\right]^{-1} \left(\frac{h}{a}\right)_{cr} \frac{d}{\dot{S}_f} \tag{4}$$

Model A

If the particle pulls free of the binder when leaving the surface, it must leave a layer of binder material under it, which must be ablated away before the process can repeat itself. The total time for one complete cycle is $(\Delta t)_{SA}$; from Eqs. (2) and (4):

$$(\Delta t)_{SA} = (\Delta t)_{cr} + (\Delta t)_A = b/\dot{S} \tag{5}$$

The average thermomechanical-erosion rate is

$$(\dot{m}_{me})_A = [(\Delta t)_{SA} b^2]^{-1}(d - \Delta S_f)d^2\rho_f \tag{6}$$

Combining Eqs. (1–6) and mass-balanced relation, then yields:

$$f_A = \frac{(\dot{m}_{me})_A}{\dot{m}_{ch}} = \left[\frac{\rho_f}{\rho_b} + \left(\frac{h}{a}\right)_{cr} - 1\right]^{-1} \frac{\rho_f}{\rho_b}\left(\frac{\rho_s}{\rho_b} - 1\right) \tag{7}$$

Model B

The analysis for this model proceeds similarly to that for model A from Eqs. (5–7), but now the total time for one complete cycle is $(\Delta t)_{sb}$

$$\because (\Delta t)_{sb} = (\Delta t)_{cr} + \frac{b - d}{S} \tag{8}$$

$$\therefore f_B = \frac{(\dot{m}_{me})_B}{\dot{m}_{ch}} = \left\{\frac{b}{d}\frac{\rho_f}{\rho_b}\left(\frac{\rho_s}{\rho_b} - 1\right) + \left[\left(\frac{\rho_f}{\rho_b} - 1\right) - \frac{b}{d}\left(\frac{\rho_s}{\rho_b} - 1\right)\right]\left(1 - \left(\frac{h}{a}\right)_{cr}\right)\right\} \div \left\{\left(\frac{h}{a}\right)_{cr}\frac{\rho_f}{\rho_b} + \left(\frac{b}{d} - 1\right)\left[\left(\frac{h}{a}\right)_{cr} + \frac{\rho_f}{\rho_b} - 1\right]\right\} \tag{9}$$

It is assumed that mechanical erosion is principally the result of aerodynamic forces acting on protruding particles. The aerodynamic forces are primarily from surface pressure gradient and rough surface shear, and that rough surface shear is almost entirely because of the drag exerted on individual protuberances. In the following, a simple expression for rough surface skin friction is first developed from published data, and then an idealized model of a protuberant particle is used to derive an equation for the mechanically eroded fraction.

A brief review of the virgin material microstructure will suggest the probable size and spacing of typical particles, assuming particle size and spacing are d and b, respectively. Figure 1 shows the resulting situation, highly idealized, in that the particle taken is a cube, with its faces oriented parallel to the principal planes of the boundary-layer coordinate system. The reaction force is shown acting at the surface of porous matrix, and the resulting overturning moment is assumed to be resisted by normal forces linearly distributed over the embedded face. The value of the overturning moment is

$$M = \tfrac{2}{3}Q(\Delta S_b - \Delta S_f) - \tfrac{1}{2}P'd^2(\Delta S_b - \Delta S_f)^2 \tag{10}$$

where $P' = \mathrm{d}p/\mathrm{d}x$ (i.e., streamwise pressure gradient).

Assuming that rough wall skin friction is entirely the result of protuberance drag, the drag force on each protuberance is

$$Q = \tfrac{1}{2}C_f\rho_e u_e^2 b^2 \tag{11}$$

Schlichting[4] gives, for the coefficient of local skin friction on a rough plate in compressible flow,

$$C_f = [2.87 + 1.58\log(x/h_s)]^{-2.5}(\rho_w/\rho_e) \tag{12}$$

The simpler expression

$$C_f = 0.027(h_s/x)^{0.2}(\rho_w/\rho_e) \tag{13}$$

matches Eq. (12) within 9% over the range $10^2 < x/h < 10^6$ and will be used here. Schlichting also gives data showing how h_s is affected by protuberance height h and spacing b for a number of protuberance element shapes, including spheres, spherical segments, cones, and short angles. Except for the data for short angles, which have very large equivalent sand roughness, and two points for spheres with b/h ratios less than 1.5, the data are well represented by the equation

$$h_s/h = 16(h/b)^{1.8}$$

substituting this in Eq. (13) gives

$$C_f = 0.047(\rho_w/\rho_e)(h/x)^{0.2}(h/b)^{0.36} \tag{14}$$

combining this with Eq. (11)

$$Q = 0.0235\rho_w u_e^2(b^{1.64}h^{0.56}/x^{0.2}) \tag{15}$$

The maximum resulting tensile stress on the particle–matrix interface is

$$\sigma_m = 6M/d^3 \tag{16}$$

This is the average stress on a microscopic scale. Viewed microscopically, the particle may be attached to the binder over only a portion of its surface. Therefore, the maximum tensile stress on a microscopic scale is

$$\sigma_m = 6M/\beta d^3 \tag{17}$$

where β is the fraction of the particle surface actually connected to the binder (viewed microscopically). Superimposed on this is the hydrostatic compressive stress arising from and equal to the local gas pressure. Thus, the net tensile stress is

$$\sigma = (6M/\beta d^3) - P \tag{18}$$

where $P = (R/\bar{M})\rho T$.

Combining this with Eqs. (10) and (15) gives the relationship between the recession of the matrix ΔS_b and the stress σ. Assuming that the particle is removed when σ exceeds the ultimate strength of the bound between the particle and the surrounding matrix, the equation can be rewritten with, $\sigma = \sigma_u$, $\Delta S_b = \Delta S_{bu}$, as follows:

$$G\left(\frac{\Delta S_{bu}}{d}\right)^2 + F\left(\frac{\Delta S_{bu}}{d}\right)^{1.56} = 1 + \frac{P}{\sigma_u} \tag{19}$$

where F and G, the dimensionless skin fraction and dimensionless pressure gradient, respectively, are defined by

$$F = \frac{\rho_w u_e^2}{x^{0.2}} \div \left[\beta\sigma_u^{1.44} \div 0.094d^{1.64}\left(1 - \frac{\rho_b}{\rho_f}\right)^{1.56}\right] \tag{20}$$

$$G = -P' \div \left[\beta\sigma_u \div 3d\left(1 - \frac{\rho_b}{\rho_f}\right)^2\right] \tag{21}$$

Equation (19) can be solved, to any desired degree of accuracy, by the method of successive approximations. An approximation that is accurate to within 5% for possible value of G and $F(G + F) > 1$ is

$$\frac{\Delta S_{bu}}{d} = \left\{\left(1 + \frac{P}{\sigma_u}\right)^{1.28} \div \left[G\left(1 + \frac{P}{\sigma_u}\right)^{0.28} + F^{1.28}\right]\right\}^{0.5} \tag{22}$$

assuming

$$H = \left(1 + \frac{P}{\sigma_u}\right)^{1.28} \div \left[G\left(1 + \frac{P}{\sigma_u}\right)^{0.28} + F^{1.28}\right] \tag{23}$$

with Eqs. (3), (4), (22), and (23) then yields the expression:

$$\left(\frac{h}{a}\right)_{cr} = H\left(\frac{\rho_f}{\rho_b} - 1\right)\Big/\left(\frac{\rho_f}{\rho_b} - H\right) \tag{24}$$

Inserting Eq. (24) into Eqs. (7) and (9) then yields

$$f_A = \frac{\rho_f}{\rho_b}\left(\frac{\rho_s}{\rho_b} - 1\right) \Big/ \left[\frac{\rho_f}{\rho_b} + H\left(\frac{\rho_f}{\rho_b} - 1\right) \div \left(\frac{\rho_f}{\rho_b} - H\right) - 1\right] \tag{25}$$

assuming

$$K = \left(\frac{\rho_f}{\rho_b} - H\right)^{-1} H\left(\frac{\rho_f}{\rho_b} - 1\right) \tag{26}$$

$$f_B = \left\{\frac{b}{d}\frac{\rho_f}{\rho_b}\left(\frac{\rho_s}{\rho_b} - 1\right) + \left[\left(\frac{\rho_f}{\rho_b} - 1\right) - \frac{b}{d}\left(\frac{\rho_f}{\rho_b} - 1\right)(1 - K)\right]\right\} \div \left[\frac{\rho_f}{\rho_b} H\left(\frac{\rho_f}{\rho_b} - 1\right) \Big/ \left(\frac{\rho_f}{\rho_b} - H\right) + \left(\frac{b}{d} - 1\right)\left(\frac{\rho_f}{\rho_b} + K - 1\right)\right] \tag{27}$$

Calculate Examples and Analysis of Result

For the validity of a theoretical analytical method a computational example is given. Parameters of ballistic missile reentry with several different physical characters are calculated. The partial calculated results are given in Figs. 2–5. It is known from Fig. 2 that total mass loss rate $\dot{m}_{t0}$ calculated by model B is greater than that by model A for certain $(h/a)_{cr}$ (i.e., $\dot{m}_{t0B} > \dot{m}_{t0A}$).

The calculation results are correct because model A is of net particle erosion and model B is of simultaneous erosion of the particle and binder around it. The change trend for models A and B is also correct because of increases in value accompanied by increments of $(h/a)_{cr}$. It is known from Fig. 3 that the mass loss rate of mechanical erosion $\dot{m}_{me}$ increases when accompanied by increments of stagnation point pressure P_s at a fixed position x. On the condition of the same stagnation point pressure, $\dot{m}_{me}$ increases accompanied by increments of x because of the operation along pressure gradient. Beyond the position x = 10 cm, $\dot{m}_{me}$ decreases accompanied by increments of the position x because of the operation against pressure gradient. These calculation results are correct and rational. The calculation results of $\dot{m}_{me}$ fairly agree with the experimental results of Ref. 7 at four values of P_s in the region of stagnation point (i.e., P_s = 80, 60, 25, and 15 atm). The five curves shown in Fig. 4 are obtained by calculation and assumption of five different values of β at certain values of P_s and b. Figure 4 shows that the mass loss rate of mechanical erosion increases accompanied by decrement of value β for fixed dimension of particle (i.e., d has same value). This calculation result is also correct. It is easy to understand in physics as the high value of β denotes a big fraction of the particle surface actually connected to the binder, and so it is not easily eroded. Figure 4 also shows that $\dot{m}_{me}/\dot{m}_{ch}$ declines when accompanied by increments of particle dimension d for certain values of b, P_s, and β. When d increases to a certain value, $\dot{m}_{me}/\dot{m}_{ch}$ equals zero to denote no existence of mechanical erosion. It is rational

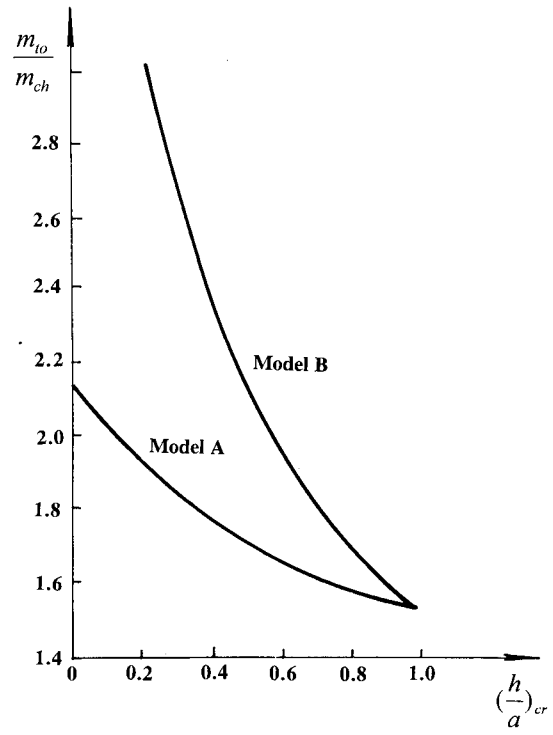

Fig. 2 Ratio of total thermochemical mass transfer parameter function of $(h/a)_{cr}$.

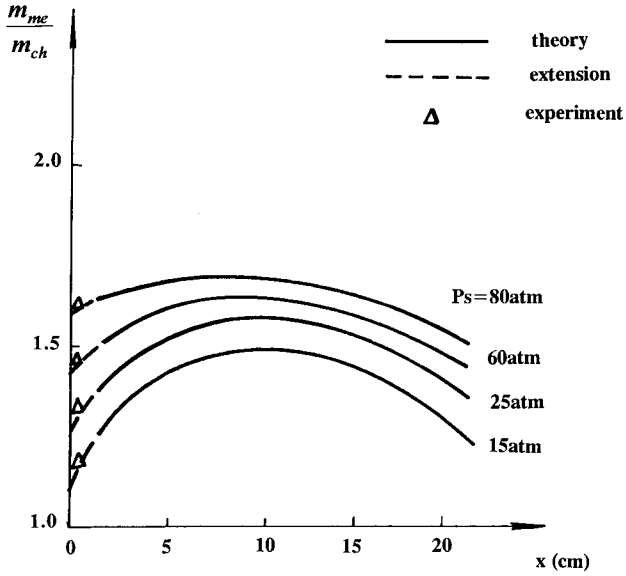

Fig. 3 Variation of m_{me}/m_{ch} with x.

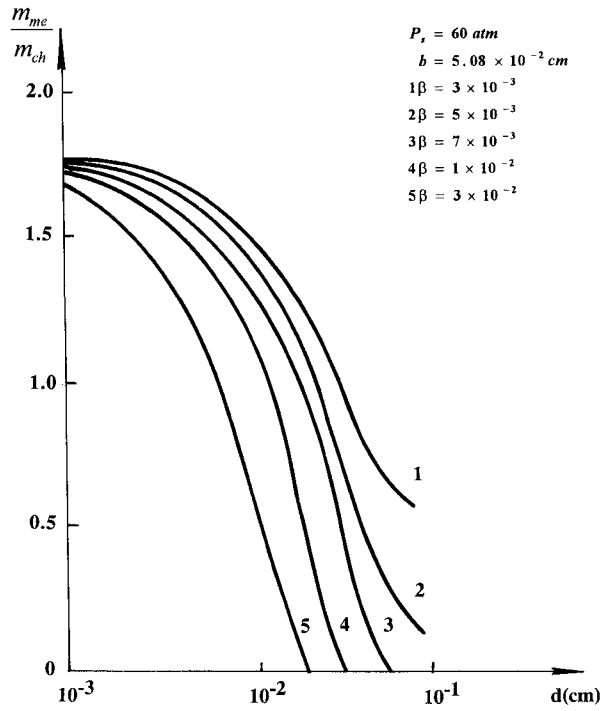

Fig. 4 Variation of m_{me}/m_{ch} with particle size.

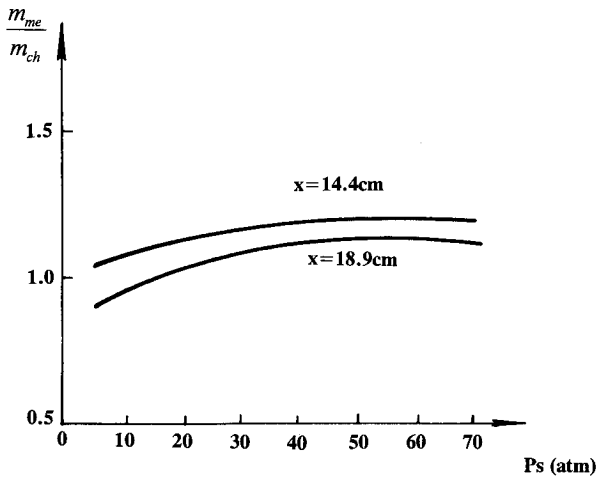

Fig. 5 Variation of m_{me}/m_{ch} with stagnation pressure.

in a physical model, but the process of actual material is unobtained. We can make a theoretical inquiry on it. It is valuable for application to develop these good ablative performances of material. Figure 5 shows two curves of $\dot{m}_{me}/\dot{m}_{ch}$ at $x = 14.4$ cm and $x = 18.9$ cm that change when accompanied by P_s, and $\dot{m}_{me}/\dot{m}_{ch}$ increases when accompanied by increments of P_s, the curve at $x = 14.4$ cm is over the curve at $x = 18.9$ cm. These change laws are all correct.

Conclusions

From the previous results of the analyses of calculation examples we can derive the following conclusions:

1) The theoretical analysis for the mechanical erosion of carbon-base materials based on a nondimensional critical roughness is dependable and accurate.

2) The theoretical results agree fairly with the experimental data. The total error is less than 10%, including 5% approximate error of Eq. (19).

3) The important parameters in this analytical method are independent of the test.

4) The analysis procedure is developed for graphite; it is generally applicable to carbon-base ablative materials, such as three-dimensionally carbon–carbon materials and carbon–phenolic composite materials.

References

[1]Ziering, M., and DiCriststina, V., "Thermomechanical Erosion of Ablative Plastic Composites," AIAA Paper 72-299, June 1972.

[2]Dolton, T. A., Maurer, R. E., and Goldstein, H. E., "Thermodynamic Performance of Carbon in Hyperthermal Environments," AIAA Paper 68-754, June 1968.

[3]McVey, D. F., Aucrbach, I., and McBride, D. D., "Some Observations on the Influence of Graphite Microstructure on Ablation Performance," AIAA Paper 70-155, Jan. 1970.

[4]Schlicting, H., "Boundary Layer Theory," 7th ed., McGraw–Hill, New York, 1979, pp. 652–654.

[5]Maahs, H. G., "Ablation Performance of Glass Like Carbons; Pyrolytic Graphite; and Artificial Graphite in the Stagnation Pressure Range 0.035–15 atm," NASA TN-D7005, 1970.

[6]Lundell, J. H., "Ablation of ATJ Graphite at High Temperatures," *AIAA Journal*, Vol. 11, No. 2, 1973, pp. 216–222.

[7]Kratsch, K. M., Martiner, M. R., Clayton, F. I., Greene, R. B., and Wuerer, J. E., "Graphite Ablation in High Pressure Environments," AIAA Paper 68-1153, Dec. 1968.